Thermodynamic Analysis of the Structural Stability of Phage 434 Cro Protein[†]

S. Padmanabhan,*[,‡] D. V. Laurents,[‡] A. M. Fernández,[§] M. Elias-Arnanz,[||] J. Ruiz-Sanz,[§] P. L. Mateo,[§] M. Rico,*[,‡] and V. V. Filimonov[§,⊥]

Instituto de Estructura de la Materia, Consejo Superior de Investigaciones Cientificas, Serrano 119, 28006 Madrid, Spain, Departamento de Química-Física, Facultad de Ciencias, Universidad de Granada, 18071 Granada, Spain, Departamento de Genética, Facultad de Biologías, Universidad de Murcia, 30071 Murcia, Spain, and Institute of Protein Research of the Russian Academy of Sciences, Puschino, Moscow Region 142292, Russia

Received July 28, 1999; Revised Manuscript Received September 24, 1999

ABSTRACT: Thermodynamic parameters describing the phage 434 Cro protein have been determined by calorimetry and, independently, by far-UV circular dichroism (CD) measurements of isothermal urea denaturations and thermal denaturations at fixed urea concentrations. These equilibrium unfolding transitions are adequately described by the two-state model. The far-UV CD denaturation data yield average temperature-independent values of 0.99 ± 0.10 kcal mol^{-1} M^{-1} for m and 0.98 ± 0.05 kcal mol^{-1} K^{-1} for $\Delta C_{p,U}$, the heat capacity change accompanying unfolding. Calorimetric data yield a temperature-independent $\Delta C_{p,U}$ of 0.95 ± 0.30 kcal mol^{-1} K^{-1} or a temperature-dependent value of 1.00 ± 0.10 kcal mol^{-1} K^{-1} at 25 °C. $\Delta C_{p,U}$ and m determined for 434 Cro are in accord with values predicted using known empirical correlations with structure. The free energy of unfolding is pH-dependent, and the protein is completely unfolded at pH 2.0 and 25 °C as judged by calorimetry or CD. The stability of 434 Cro is lower than those observed for the structurally similar N-terminal domain of the repressor of phage 434 (R1−69) or of phage λ (λ_{6-85}), but is close to the value reported for the putative monomeric λ Cro. Since a protein's structural stability is important in determining its intracellular stability and turnover, the stability of Cro relative to the repressor could be a key component of the regulatory circuit controlling the levels and, consequently, the functions of the two proteins in vivo.

An understanding of the physical interactions underlying the structure, folding, and function of a protein requires a complete thermodynamic description of its conformational stability. Such a description relies on quantitative analyses of thermally or chemically induced folding−unfolding transitions (monitored by calorimetry or spectroscopically), followed by a data extrapolation to given conditions of temperature, pH, etc. To extrapolate thermal denaturation data, the change in heat capacity ($\Delta C_{p,U}$) and its temperature dependence must be known. These are best determined by calorimetry, although other methods have also been developed. Extrapolation of data from chemical denaturation (e.g., urea and guanidine hydrochloride) is based either on the linear free energy model (LEM)[1] found to be valid for a number of proteins (*1*, *2*) or on the denaturant−protein binding model (DBM) (*3*, *4*). Combined analyses of chemical and thermal denaturation data which assume a temperature-independent $\Delta C_{p,U}$ and the thermodynamic equivalence of thermally and chemically denatured states have been reported for various proteins (*2*, *5*−*12*).

The conformational stability and the principal thermodynamic parameters (ΔG_U, ΔH_U, ΔS_U, T_m, and $\Delta C_{p,U}$) which describe the folding transitions of bacteriophage 434 Cro protein are examined here. In vivo, Cro and the repressor proteins regulate the switch between phage lysis and lysogeny by sequence-specific DNA binding (*13*). 434 Cro has several properties that are desirable for physical studies of thermodynamic stability and of structure−stability correlations. It is a small (71-residue) single-domain protein with no disulfides or prosthetic groups that is highly soluble and monomeric in aqueous solutions and whose three-dimensional crystal (*14*) and solution structures (*15*) are known. Its single domain consists of five α-helices whose folding topology resembles remarkably those observed for the 69-residue N-terminal domain of phage 434 repressor (R1−69), and for the 85 residues of the N-terminal domain of phage λ repressor (*14*−*17*), and so they constitute a family of proteins that are suitable for comparitive studies of folding, stability, and specific DNA binding. A reversible two-state folding behavior involving only native and unfolded states without any intermediate conformations is observed for 434 Cro under equilibrium conditions (*15*), and has been reported for λ_{6-85} (residues 6−85 of the λ repressor N-terminal

[†] Supported by grants from DGICYT (Spain) [PB93-0189 (to M.R.) and PB96-1446 (to P.L.M.)] and the European Community [B104-CT97-2086 (to M.R.) and INTAS 93-007 and CT96-0013 (to P.L.M. and V.V.F.)]. D.V.L. is a Leukemia Society of America (U.S.A.) postdoctoral fellow.

* Corresponding authors. E-mail: padhu@malika.iem.csic.es and rico@malika.iem.csic.es. Fax: 34-1-564 2431.

[‡] Consejo Superior de Investigaciones Cientificas.

[§] Universidad de Granada.

[||] Universidad de Murcia.

[⊥] Institute of Protein Research of the Russian Academy of Sciences.

[1] Abbreviations: CD, circular dichroism; DBM, denaturant binding model; DSC, differential scanning calorimetry; GdnHCl, guanidine hydrochloride; DTT, 1,4-dithiothreitol; ITC, isothermal titration calorimetry; λ_{6-85}, residues 6−85 of the N-terminal domain of the λ repressor; LEM, linear extrapolation model; NMR, nuclear magnetic resonance; R1−69, residues 1−69 of the N-terminal DNA-binding domain of the 434 repressor.

10.1021/bi991757+ CCC: $18.00
Published on Web 11/04/1999

domain; *9*, *18*) and R1−69 (*19*). The available thermodynamic parameters that define the folding of λ_{6-85} and R1−69 are compared with those determined for 434 Cro in this study, and their possible implications on the folding and the biological roles of these proteins are discussed.

MATERIALS AND METHODS

Preparation of Protein

A plasmid containing the gene for 434 Cro under the control of a *tac* promoter (pRW74) was initially used to overexpress and purify the protein as reported previously (*15*). To enhance the protein yield, the gene was recloned into the T7 promoter-based pET11b expression system (*20*). A PCR-amplified fragment containing the 434 Cro gene with its initiator ATG codon forming the end of an *Nde*I restriction site and the TAA stop codon followed by a *Bam*HI site was generated using the plasmid pRW74 as a template, purified (Promega Wizard kit), and then cloned into the *Nde*I and *Bam*HI sites of the plasmid pET11b. The construct was verified by DNA sequencing (DNA sequencing facility of CIB-Madrid). To express the 434 Cro protein, *Escherichia coli* strain BL21(DE3) was transformed with the plasmid, grown to late logarithmic phase, and then induced with 0.4 mM isopropyl β-D-thiogalactoside for 5 h at 37 °C or overnight at 25 °C. The cells were then harvested and lysed, and the protein was purified by ion-exchange and reverse-phase HPLC as before (*15*). The protein purity was verified in a 15% SDS−PAGE gel with Coomasie blue staining and by HPLC in a Vydac-C_4 reverse-phase column. The absorbance at 280 nm was used to determine protein concentration using an ϵ_{280} of 6970 M^{-1} cm^{-1} in 6 M guanidinium hydrochloride (ultrapure from ICN Biomedicals) or 6370 M^{-1} cm^{-1} under native conditions (determined as described in refs *21* and *22*).

CD Measurements

CD measurements were performed in a Jasco J720 spectropolarimeter equipped with a Neslab temperature control circulating water-bath unit. Thermal and urea unfolding transitions were monitored by the far-UV CD signal at 222 nm using protein concentrations of 10−20 μM and in the presence of 100 mM KCl, 25 mM KH_2PO_4, and 1 mM DTT and at pH 6.0. The solution pH measured at room temperature was used without further corrections for temperature effects. Each unfolding experiment was carried out two or more times, and the data were combined and then analyzed. CD spectra were collected using a 1 or 2 mm path length cuvette at a rate of 20 nm/min, a bandwidth of 1 nm, and a 2−4 s response time and averaged over six scans. Thermal unfolding curves were obtained using a heating rate of 20 °C/h. The cuvette temperature was calibrated using an external thermocouple thermometer. To minimize the amount of protein used and also the errors associated with preparing individual samples, urea denaturations were carried out by serial addition to the protein of sample small aliquots of a concentrated stock solution of urea (ultrapure from ICN Biomedicals) prepared using the protocol described by Pace et al. (*23*). After each addition of urea, the cuvette capped with a Teflon stopper was inverted repeatedly to ensure complete mixing and then allowed to reach thermal and chemical equilibrium in the CD instrument for at least 5 min before data were recorded. Under the experimental conditions that were used, the unfolding transitions are reversible as verified by the temperature scan obtained for a sample coinciding with a second scan for the same sample cooled immediately after the first scan, and from the mean residue ellipticity at 222 nm, $[\Theta]_{222}$ (in deg cm^2 $dmol^{-1}$), of a sample at a given urea concentration being the same irrespective of whether the sample at a given urea concentration was prepared by the addition of urea or by diluting the sample with a high level of urea. The equilibrium was achieved rapidly as seen by the rapid recovery of the initial CD signal on cooling for thermal transitions and the CD signal being unchanged on equilibrating a sample after addition of urea for a few minutes or overnight.

Calorimetry

Differential scanning calorimetry (DSC) and isothermal titration calorimetry (ITC) data were obtained in a MicroCal VP-DSC calorimeter and in an ITC unit of the Microcal System (MicroCal Inc.). Samples for calorimetry were prepared by dissolving the lyophilized protein in the desired buffer followed by filtering and dialyzing overnight against the same buffer. The buffers that were used contained 100 mM KCl and 20 or 25 mM sodium glycine or acetate or phosphate depending upon the desired pH (pH 2.0, 2.65, 3.0, 4.0, 4.5, and 6.0). No corrections were made for temperature effects on pH. Samples were saturated with nitrogen to minimize oxidation of the single Cys present in 434 Cro which can lead to oligomerization and the consequent irreversible transitions. In DSC measurements, the samples were routinely heated to 375 K using scan rates of 60 or 90 K/h, cooled slowly in the calorimeter, and reheated to check the reversibility of folding. The sample volumes in DSC experiments were 0.52 mL with protein concentrations of around 100−200 μM. A molecular mass, M_r, of 8060 Da and a partial specific volume of 0.753 mL/g (*15*) were used in transforming calorimetric data to temperature-dependent partial molar heat capacities and were then subjected to single- and multiple-fitting procedures based on the equations described elsewhere (*24*−*26*) using SigmaPlot 4.0 software (Jandel). ITC data were acquired at 15 and 25 °C, the cell volume being 1.348 mL. Three injections each of 30 μL of a 0.427 mM protein solution in 5 mM potassium acetate (pH 5.0) (buffer A) were made into the calorimetric cell containing buffer B (20 mM phosphate) or buffer C (20 mM glycine) at pH 2.0, the final protein concentration being 27 μM. In separate control experiments, the same three pulses of 30 μL of buffer A without protein were injected into the cell filled with buffer B or C to determine the heats of mixing for the buffers alone: −160 and 300 μcal for buffer B and C, respectively, mixing with buffer A. These were subtracted from the heats of protein transfer to pH 2.0 and then corrected for the heats of ionization (*27*) to determine the unfolding enthalpy. The pHs of the mixture measured at the end of the experiment were 2.0 and 2.2 for the phosphate and glycine buffers, respectively.

Data Analysis

Analysis of Far-UV CD Denaturation Data. Far-UV CD thermal and urea denaturation data were analyzed using the

two-state model for the native (N) to denatured (U) equilibrium (N ⇔ U) with an apparent equilibrium constant K_U (=[U]/[N] = f_U/f_N). f_U and f_N are the fractions of denatured and native protein, respectively, at a given temperature or urea concentration ($f_U + f_N = 1$). The free energy of unfolding at temperature T (in kelvin), $\Delta G_U(T)$ (=$-RT \ln K_U$, R being the universal gas constant), and the observed CD signal, θ, are related as follows (see refs *7*−*12* and *15*):

$$\theta = \frac{\theta_N + \theta_U \exp(-\Delta G_U/RT)}{[1 + \exp(-\Delta G_U/RT)]} \quad (1)$$

where θ_N and θ_U are the signals for the fully native and fully unfolded states, respectively ("baselines"), and correspond to the pre- and post-transition zone plateau regions. They are usually described as linear functions of temperature (t in degrees Celsius) and urea concentration, [Ur] (*7*):

$$\theta_N(t,[Ur]) = \theta_N{}^0 + a_{N0}t + b_{N0}[Ur] \quad (2)$$

$$\theta_U(t,[Ur]) = \theta_U{}^0 + a_{U0}t + b_{U0}[Ur] \quad (3)$$

where θ^0 are the intercepts and a_0 and b_0 values the temperature- and urea-dependent terms, respectively.

The urea dependence of ΔG_U in isothermal urea denaturations described by the linear extrapolation model (LEM) (*1*, *2*, *28*) is

$$\Delta G_U(T,[Ur]) = \Delta G_U(T,0) - m[Ur] \quad (4a)$$

The free energy of unfolding at T and zero urea $\Delta G_U(T,0) = mC_m$, where C_m is the urea concentration at the midpoint of the folding transition where $\Delta G_U(T,[Ur])$ is zero.

The denaturant binding model (DBM) (*3*, *4*) for isothermal urea denaturation yields

$$\Delta G_U(T,[Ur]) = \Delta G_U(T,0) - RT\Delta n \ln(1 + ka) \quad (4b)$$

where Δn is the change in the number of urea binding sites upon unfolding, k the binding affinity of protein for urea, and a the molar activity of urea. k, a, and urea activity coefficients used in this study are from Makhadatze and Privalov (*4*) or from their data fitted to temperature- and urea concentration-dependent polynomials (as in ref *10*).

The temperature dependences of $\Delta G_U(T,[Ur])$, the enthalpy ($\Delta H_m'$), and the entropy ($\Delta S_U'$) can be expressed as (*29*)

$$\Delta G_U(T,[Ur]) = \Delta H_U'(T) - T\Delta S_U'(T) = \Delta H_m'(1 - T/T_m') - \Delta C_{p,U}' \times [(T_m' - T) + T \ln(T/T_m')] \quad (5)$$

$$\Delta H_U'(T,[Ur]) = \Delta H_m' + \Delta C_{p,U}'(T - T_m') \quad (6)$$

$$\Delta S_U'(T,[Ur]) = \Delta H_m'/T_m' + \Delta C_{p,U}' \ln(T/T_m') \quad (7)$$

where T_m' is the temperature (in kelvin) at the midpoint of the folding transition where $\Delta G_U = 0$, $\Delta H_m'$ the enthalpy at T_m', and $\Delta C_{p,U}'$ the heat capacity increment assumed to be independent of temperature (the primes indicate values in the presence of urea). This $\Delta C_{p,U}'$ can be extracted from combined thermal and urea denaturation data using different procedures that assume a two-state unfolding transition (*5*−*12*) or from calorimetry (see below). Data for each equilibrium unfolding experiment were obtained at least in duplicate, combined, and then fit to the appropriate equations listed above using Kaleidagraph (Synergy Software, PCS Inc.) or Sigmaplot for Windows (Jandel) software. The errors listed are those reported by these fitting algorithms.

Additional thermodynamic parameters, T_h where $\Delta H_U = 0$, T_s where $\Delta S_U = 0$ and where the protein has maximum stability, and $T_m{}^c$, the transition temperature for cold denaturation, can be obtained using the following expressions (*29*, *30*):

$$T_h = T_m - (\Delta H_m/\Delta C_{p,U}) \quad (8)$$

$$T_s = T_m \exp(-\Delta S_m/\Delta C_{p,U}) = T_m \exp[-\Delta H_m/(T_m\Delta C_{p,U})] \quad (9)$$

$$\Delta G_U(\max) = \Delta H_m + \Delta C_{p,U}(T_s - T_m) = \Delta C_{p,U}(T_s - T_h) \quad (10)$$

Analysis of Calorimetry Data. DSC curves were fit to equations that could be applied to the two-state transition model. Two different approaches were used to define ΔH_U and ΔS_U: (a) in terms of ΔH_m and T_m (eqs 5−7, [Ur] = 0) as described in detail elsewhere (*24*−*26*, *31*) or (b) in terms of T_h and T_s (eqs 8−10) as described below. Both approaches were used for individual or multiple-curve fitting under the assumption that $\Delta C_{p,U}$ is temperature-dependent since, from a consideration of the calorimetric curves, it is clear that $C_{p,N}(T)$ and $C_{p,U}(T)$ have different slopes so that $\Delta C_{p,U}$ is not constant but decreases with temperature in the transition temperature range. For simplicity, $C_{p,N}(T)$ and $C_{p,U}(T)$ were assumed to be linear functions of temperature in most fittings.

$$C_{p,N}(T) = a_{N,r} + b_{N,r}(T - T_r) \quad (11a)$$

$$C_{p,U}(T) = a_{U,r} + b_{U,r}(T - T_r) \quad (11b)$$

$$\Delta C_{p,U}(T) = \Delta a_{U,r} + \Delta b_{U,r}(T - T_r) \quad (12)$$

where a and b are constants and T_r is any selected reference temperature. Thus, when $T_r = T_h$, the following may be derived (*25*):

$$\Delta H_U(T) = \Delta a_{U,h}(T - T_h) + (^1/_2)\Delta b_{U,h}(T - T_h)^2 \quad (13)$$

$$\Delta S_U(T) = (\Delta a_{U,h} - \Delta b_{U,h}T_h) \ln(T/T_s) + \Delta b_{U,h}(T - T_s) \quad (14)$$

$$K_U(T) = \exp[\Delta S_U(T)/R - \Delta H_U(T)/RT] \quad (15)$$

$$C_p(T) = C_{p,N} + \Delta C_{p,U}K_U/(1 + K_U) + (K_U/R)[\Delta H_U/T(1 + K_U)]^2 \quad (16)$$

For each DSC curve, instead of the usual six adjustable parameters, ΔH_m, T_m, Δa_U, Δb_U, Δa_N, and Δb_N (*24*, *25*), six others corresponding to T_h, T_s, $\Delta a_{U,h}$, $\Delta b_{U,h}$, $a_{N,h}$, and $b_{N,h}$ are used in the fittings. Using T_s and T_h instead of ΔH_m and T_m is more appropriate for 434 Cro since for some solvent conditions $\Delta G_U(T_m) \neq 0$ but is negative at all temperatures ($\Delta G_U < 0$ and $f_N < 0.5$ for pH <3.0). The T_h/T_s fitting procedure was used in the simultaneous fitting of the averaged melting curves measured for pH 2.65, 3.0, 3.5, 3.75, 4.0, 4.5, and 5 assuming that b_N, $\Delta C_{p,U}$, and T_h were the

same for all the data sets, while $a_{N,h}$ and T_s were adjusted for each curve (making $a_{N,h}$ adjustable allows the curve positions along the C_p axis to be aligned). Thus, for the set of seven different curves, we have 17 adjustable parameters ($3 + 7 \times 2$).

It is known that at least $C_{p,U}$ can be a nonlinear function of temperature (*32*, *40*). So the curves for pH >3.5 were subjected to fittings where $C_{p,U}$ and $C_{p,N}$ were assumed to have quadratic temperature dependences to check if nonlinear baselines improve the quality of the fit. For simplicity, the coefficient for the quadratic term is assumed to be the same for both $C_{p,U}$ and $C_{p,N}$ so that the heat capacity increment, $\Delta C_{p,U}$, is again defined by eq 12. Thus,

$$C_{p,N}(T) = a_{N,h} + b_{N,h}(T - T_h) + c_N(T - T_h)^2 \quad (17a)$$

$$C_{p,U}(T) = a_{U,h} + b_{U,h}(T - T_h) + c_N(T - T_h)^2 \quad (17b)$$

The ITC data were corrected for the heats of dilution and further analyzed using the following equations:

$$\Delta H_{tot} = \Delta H_U + \Delta H_{i,prot} + \Delta H_{i,phos} \quad (18a)$$

$$\Delta H_{tot} = \Delta H_U + \Delta H_{i,prot} + \Delta H_{i,gly} \quad (18b)$$

$$\Delta\Delta H_{tot} = (\Delta H_{i,phos} - \Delta H_{i,gly}) = p(\Delta h_{i,phos} - \Delta h_{i,gly}) \quad (19)$$

where $\Delta H_{i,prot}$, $\Delta H_{i,phos}$, and $\Delta H_{i,gly}$ are the heats accompanying proton transfer to protein, phosphate, and glycine buffers, respectively. Δh are the heats of ionization for the phosphate and glycine COOH groups with the lowest pK values (from ref *27*) which together with the experimentally determined $\Delta\Delta H_{tot}$ provide values for p, the number of protons transferred to protein from buffer at pH 2 (phosphate or glycine). These p values and the average heat effect per proton in 434 Cro (=0.57 kcal mol^{-1}, estimated from the number of acidic groups in the protein, four Glu, one Asp, and one C-terminal carboxyl, and the reported heats of ionization for these groups; *27*) provide values for $\Delta H_{i,prot}$.

RESULTS

All the data accumulated thus far for 434 Cro, NMR, far- and near-UV CD and the intrinsic Trp fluorescence spectra, its monomeric nature over a wide concentration range (up to millimolar levels), and the coincident equilibrium unfolding curves obtained using different spectroscopic probes, are consistent with two-state folding (*15*). When monitored by the strong far-UV CD signal at 222 nm characteristic of the helices (as in 434 Cro), thermal and urea denaturation curves at pH 6.0 and the protein concentrations that were used are reversible and equilibrate rapidly between the folded and unfolded forms. Isothermal urea denaturation curves were obtained at five different constant temperatures from 5 to 25 °C. Thermal denaturations were carried out in the presence of different fixed concentrations of urea ranging from 0 to 3 M (maximum temperatures of 75−85 °C) and from 6 to 7 M (maximum temperature of 50 °C). Sample exposure to high temperatures was kept short to minimize any protein modification by urea decomposition products and consequent irreversibility (*7*).

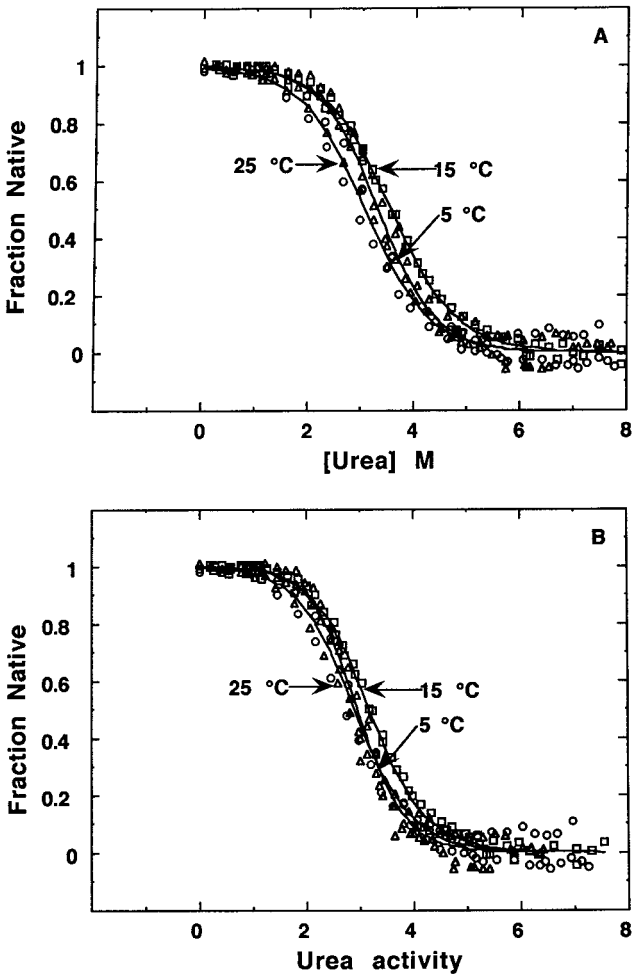

FIGURE 1: Isothermal urea denaturation data for 434 Cro at 5 (△), 15 (□), and 25 °C (○) monitored by the far-UV CD signal at 222 nm. Solution conditions are pH 6.0, 100 mM KCl, 25 mM KH_2PO_4, and 1 mM DTT. Lines are fits of the data using the parameters listed in Table 1 (see the text) for (A) the linear extrapolation model and (B) the denaturant binding model.

Isothermal Urea Denaturations by Far-UV CD. The experimental data and model fittings for urea denaturation curves at constant temperatures of 5, 15, and 25 °C plotted as the fraction of the folded protein are shown in panels A (LEM) and B (DBM) of Figure 1. The data set obtained at a given temperature was individually subjected to a six-parameter nonlinear least-squares fitting, four of which describe the native and unfolded baselines. The remaining two parameters are m and C_m or m and $\Delta G_U(T,0)$ for LEM (eq 4a), and Δn and $\Delta G_U(T,0)$ for DBM (eq 4b). In the latter, values for k, the intrinsic protein-urea binding constant, and a, the activity of urea, were separately assigned as described in Materials and Methods (note that k decreases and the urea activity increases with temperature; *4*). Table 1 lists the best-fit values obtained using the two models. m values are, within error, independent of temperature over the examined range, the average being 0.99 ± 0.09 kcal mol^{-1} M^{-1}. C_m values which are more accurately determined appear to have some temperature dependence, while $\Delta G_U(T,0)$ values, the zero-urea value at temperatures between 5 and 25 °C, range within the error of the measurement. As for some other small proteins (*7*, *10*), the change in the number of denaturant binding sites, Δn, is small and relatively invariant with temperature between 5 and 25 °C with a mean value of 35 ± 3. ΔG_U-

Table 1: Analysis of Isothermal Far-UV CD Urea Denaturation Data for 434 Cro[a]

parameter[b]	5 °C	10 °C	15 °C	20 °C	25 °C
C_m (M urea)	3.32 ± 0.08	3.31 ± 0.06	3.56 ± 0.05	3.42 ± 0.09	3.07 ± 0.15
m (kcal mol^{-1} M^{-1})	0.99 ± 0.10	1.03 ± 0.06	0.91 ± 0.05	1.01 ± 0.12	1.00 ± 0.14
$\Delta G_U(T,0)$ (kcal mol^{-1})	3.28 ± 0.38	3.40 ± 0.25	3.23 ± 0.31	3.44 ± 0.47	3.05 ± 0.49
k	0.086	0.078	0.071	0.065	0.061
Δn	33 ± 2	36 ± 2	33 ± 2	37 ± 4	37 ± 5
$\Delta G_U(T,0)$ (kcal mol^{-1})	4.12 ± 0.42	4.13 ± 0.28	3.87 ± 0.23	3.97 ± 0.50	3.52 ± 0.58

[a] Solution conditions are 100 mM KCl, 25 mM KH_2PO_4 (pH 6.0), and 1 mM DTT. [b] Estimates for C_m, m, and $\Delta G_U(T,0)$ in the first three rows were determined using the linear extrapolation model (LEM), while k, Δn, and $\Delta G_U(T,0)$ in the bottom three rows were determined using the denaturant binding model (DBM). $\Delta G_U(T,0)$ is the value at 0 M urea, and Δn is the nearest integral value (see the text).

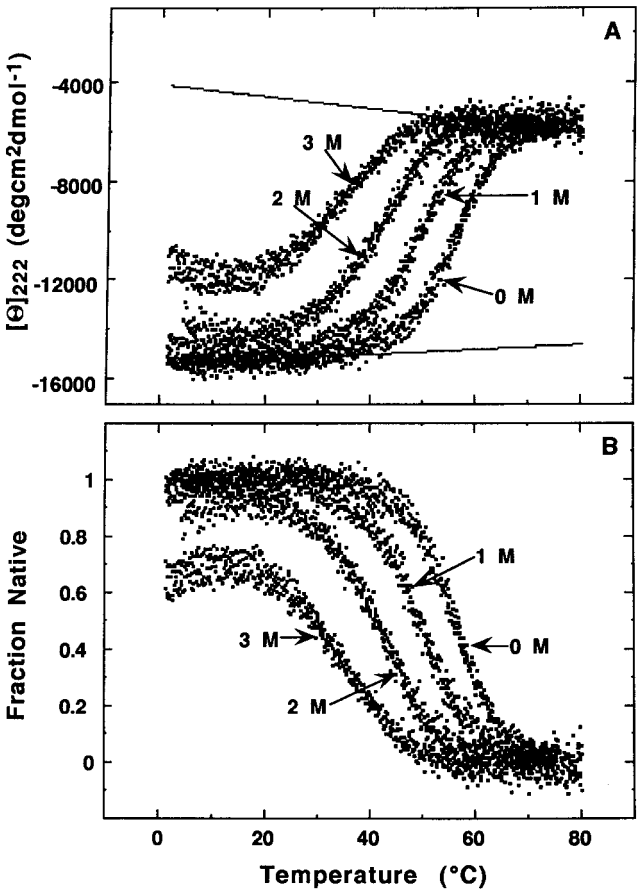

FIGURE 2: Thermally induced transitions of 434 Cro at fixed urea concentrations of 0, 1, 2, and 3 M monitored by the far-UV CD signal at 222 nm at pH 6.0, 100 mM KCl, 25 mM KH_2PO_4, and 1 mM DTT. Each curve is the composite of at least two different experiments. (A) Mean residue ellipticity, $[\Theta]_{222}$, data. The lower native baseline and the upper unfolded baseline were generated as described in the text. (B) Data depicted in panel A plotted as fraction of protein folded using the baselines shown in panel A.

(T,0) from DBM and LEM differ by about 0.5 to 0.8 kcal mol^{-1}, as observed for some other proteins (*5*, *10*, *26*).

Thermal Denaturations in Fixed Urea Concentrations by Far-UV CD. Figure 2 illustrates the effects of urea on thermostability; as the fixed urea concentration increases, high-temperature unfolding (heat denaturation) occurs at lower temperatures, and low-temperature unfolding (cold denaturation) is apparent by 3 M urea. Using different procedures (*7*), these CD thermal denaturation data were analyzed to determine $\Delta C_{p,U}$ which is assumed to be temperature-independent (even though it does vary at least to a small extent with temperature; *5*, *29*), once the folded and unfolded baselines were defined as discussed below.

The lower line in Figure 2A corresponding to the fully folded protein baseline was generated as follows. In 0 M urea, the CD data in the pretransition region (5−20 °C) are a function of temperature alone, and a linear fit provides the intercept and temperature coefficient. These were combined with the pretransition (5−20 °C) CD data obtained in the presence of <2 M urea to evaluate the coefficient for the urea-dependent term. Thus, the native baseline (eq 2) is given by the equation $\theta_N(T,[Ur]) = (-15420 \pm 36) + (10 \pm 2)t + (92 \pm 150)[Ur]$. Here θ_N is in units of deg cm^2 dmol^{-1} at 222 nm, t in degrees Celsius, and [Ur] in molar. This expression was used for all the thermal denaturation curves obtained at fixed urea concentrations, including those at 2.5 and 3 M urea where the protein is not completely folded at any temperature and the pretransition baselines are not defined. The urea-dependent term in eq 2 (or eq 3) essentially offsets the baselines by a constant amount in the thermal denaturation curves, and is small relative to the native baseline intercept value for 0−3 M urea. The CD signal at 222 nm arises principally from helical conformations and from studies with isolated helical peptides (*33*), and the temperature dependence (in degrees Celsius) of $[\Theta]_{222}$ for a 100% helical peptide of chain length N_r is given by $(-44000 + 250t)(1 - 3/N_r)$. This expression can be used to determine $[\Theta]_{222}$ for each helix in 434 Cro using as the helical length N_r as determined in the three-dimensional structure (*14*, *15*). If it is further assumed [as done previously (*12*)] that the observed $[\Theta]_{222}$ for the whole protein is a weighted sum of the $[\Theta]_{222}$ for each helix, the weight being the ratio of the number of residues in that helix to the total number in the protein, and then the temperature dependence would be predicted to be $(-16700 + 95t)$ for 434 Cro as compared to the experimental folded baseline at 0 M urea obtained above.

The upper baseline for the unfolded protein was generated using the approach described in other reports (*8*, *34*). CD data for the thermal transitions in the presence of 2.5 or 3 M urea in the post-transition region (where it is defined over a sufficiently wide temperature range) and those obtained for the fully unfolded protein at ≥6 M urea (not shown) when fit individually as linear functions of temperature yielded essentially the same slope whose mean value is −24.41 deg cm^2 dmol^{-1} K^{-1} with a standard deviation of 2.04 deg cm^2 dmol^{-1} K^{-1}. These fits are therefore parallel to one another, with a constant offset corresponding to the urea-dependent contribution in eq 3. The latter was subsumed by individually fitting the post-transition region for each thermal denaturation curve (including those for zero or low urea where this region is not defined over a sufficiently wide temperature range) as a linear function of temperature whose coefficient is set

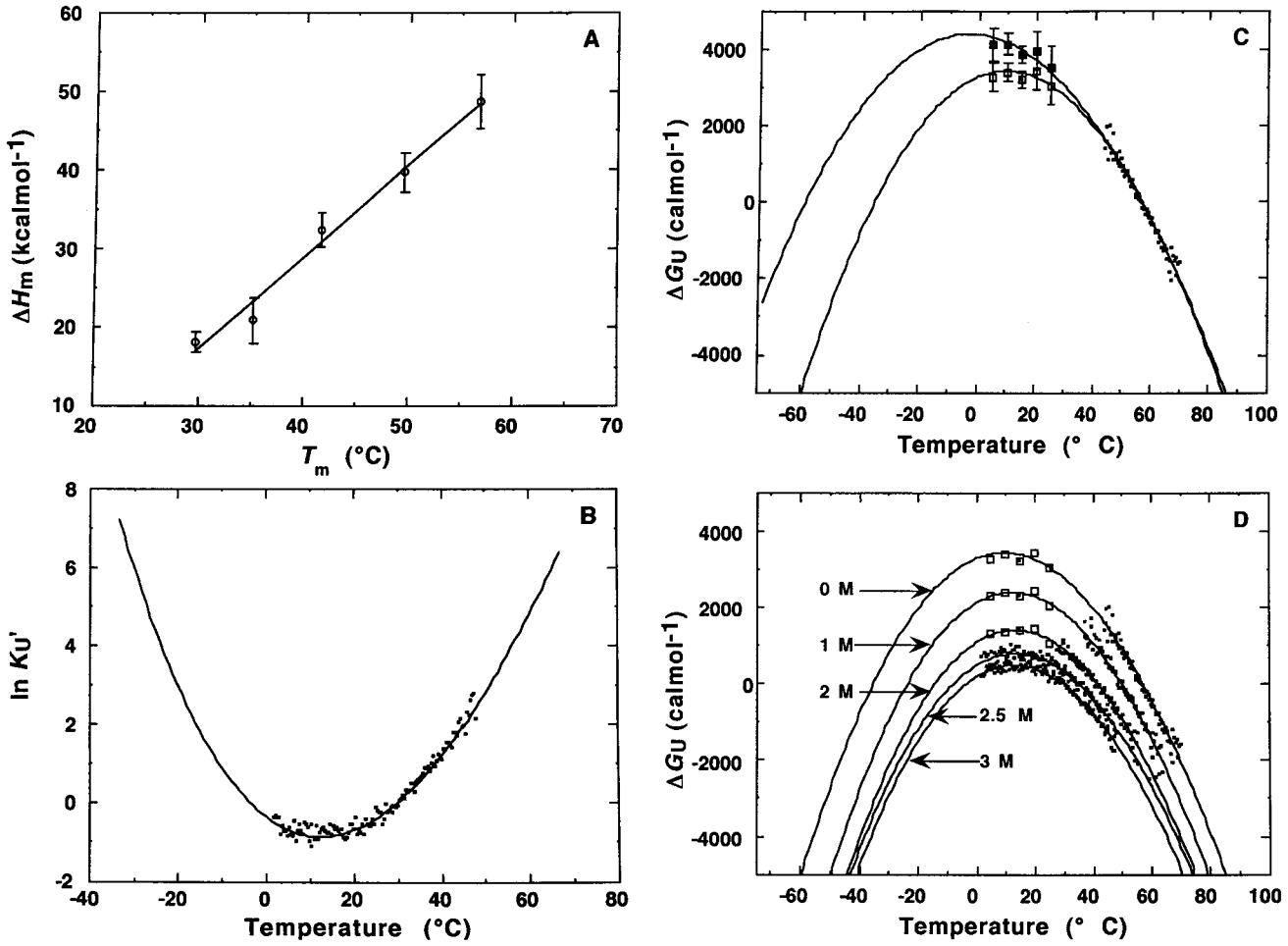

FIGURE 3: Analysis of thermal unfolding curves of 434 Cro monitored by the far-UV CD signal at 222 nm in various concentrations of urea at pH 6.0, 100 mM KCl, 25 mM KH_2PO_4, and 1 mM DTT. (A) $\Delta H_m'$ vs T_m' plot obtained by van't Hoff analysis. (B) Analysis of thermal denaturation data at 3 M urea using the method of Chen and Schellman (*34*) as described in the text. (C) Fits of ΔG_U to eq 5 using thermal denaturation data obtained in the absence of urea and isothermal urea denaturation data at lower temperatures obtained by LEM (large white squares with solid line showing the fit) or from DBM (large black squares with dotted line showing the fit) (*5*). (D) Fits (solid lines) of ΔG_U to eq 5 using the thermal denaturation data obtained in the presence of the indicated urea concentration. For 0−2 M urea, data at lower temperatures are from LEM analysis of isothermal urea denaturations (white squares). Only every fourth data point is shown for the curves in panels B−D, and the error bars are indicated only in panel C for clarity.

to the mean value indicated above to generate individual unfolded baselines.

In one procedure for analyzing the CD thermal denaturation data, $\Delta H_m'$ and T_m' at each urea concentration are estimated by a van't Hoff analysis (linear ln K_U vs $1/T$ plot) of the corresponding thermal denaturation curve over the narrow temperature range (≤5 °C) where the transition occurs ($0.4 \leq f_N \leq 0.6$). The slope of a linear plot of $\Delta H_m'$ versus T_m' is then used to evaluate $\Delta C_{p,U}'$ (*5*, *7*). Heat denaturation is essentially complete for 434 Cro for all urea concentrations examined, and a linear fit of the $\Delta H_m'$ versus T_m' data yields a $\Delta C_{p,U}'$ of 1.17 ± 0.09 kcal mol^{-1} K^{-1} (Figure 3A). This value is approximate because the analysis assumes that $\Delta H_m'$ is constant over the narrow temperature range (even though it is temperature-dependent and $\Delta C_{p,U}' \neq 0$), and since urea binding to protein has an enthalpic contribution which increases with urea and is opposite in sign from the unfolding enthalpy (*4*), $\Delta H_m'$ can differ from the true unfolding enthalpy.

In the procedure described by Chen and Schellman (*34*), a single thermal unfolding curve exhibiting both heat and cold denaturation (e.g., in 3 M urea) is fit to the equation ln $K_U' = A - A(T_m'/T) + C \ln(T_m'/T)$ derived from eq 5 with A being equal to $-[\Delta C_{p,U}' + \Delta S_U'(T_0)]/R$ and C being equal to $-\Delta C_{p,U}'/R$ (*7*, *34*). This fitting for the 3 M urea thermal denaturation data (Figure 3B) yields two T_m' values for the hot and cold denaturation transitions (29.70 ± 0.11 and −3.57 ± 0.34 °C, respectively) as long as the initial guesses for T_m' chosen in the fitting were above 60 °C or below −40 °C, with both fittings yielding the same temperature-independent $\Delta C_{p,U}'$ of 1.00 ± 0.02 kcal mol^{-1} K^{-1}.

Following the method of Pace and Laurents (*5*), $\Delta G_U(T,0)$ was determined over the entire transition region ($0.05 \leq f_N \leq 0.95$) of the thermal denaturation curve obtained in the absence of urea (indicated by dropping the primes from the thermodynamic parameters) and combined with the lower-temperature $\Delta G_U(T,0)$ determined in isothermal urea denaturations, and then the entire set was fit to eq 5 with ΔH_m, T_m, and $\Delta C_{p,U}$ as variable parameters. Figure 3C shows the data using either LEM or DBM values for the lower-temperature $\Delta G_U(T,0)$ values (Figure 1 and Table 1) and the respective fits generated using different initial guesses for T_m as discussed above. $\Delta G_U = 0$ at the two distinct temperatures (see Table 2): T_m which corresponds to heat

Table 2: Analysis of Thermal Denaturation of 434 Cro at Fixed Urea Concentrations[a]

[urea] (M)	T_m' (°C)	$T_m^{c\prime}$ (°C)[b]	$\Delta H_m'$ (kcal mol^{-1})	$\Delta H_m^{c\prime}$ (kcal mol^{-1})[b]	$\Delta C_{p,U}'$ (kcal mol^{-1} K^{-1})
0	57.0 ± 0.1	−35.5 ± 2.6	46.6 ± 0.5	−37.5 ± 0.6	0.91 ± 0.03
1	49.8 ± 0.1	−23.7 ± 3.0	40.5 ± 0.6	−34.1 ± 0.6	1.01 ± 0.05
2	41.6 ± 0.1	−14.2 ± 2.0	30.7 ± 0.3	−27.0 ± 0.3	1.03 ± 0.05
2.5	35.1 ± 0.1	−7.9 ± 0.5	21.9 ± 0.3	−19.8 ± 0.3	0.97 ± 0.02
3	29.7 ± 0.1	−3.5 ± 0.3	17.3 ± 0.2	−16.0 ± 0.2	1.00 ± 0.02

[a] The conditions are pH 6.0, 100 mM KCl, and 25 mM KH_2PO_4. [b] Cold (low-temperature) denaturation values.

denaturation with enthalpy ΔH_m and T_m^c which corresponds to cold denaturation with enthalpy ΔH_m^c for the same temperature-independent $\Delta C_{p,U}$ of 0.91 ± 0.03 kcal mol^{-1} K^{-1} when the fittings included LEM $\Delta G_U(T,0)$ or a $\Delta C_{p,U}$ of 0.71 ± 0.03 kcal mol^{-1} K^{-1} when DBM $\Delta G_U(T,0)$ values were included (Table 2). While ΔH_m and T_m for the heat denaturation are essentially identical using LEM or DBM $\Delta G_U(T,0)$ values, ΔH_m^c and T_m^c are considerably different (Figure 3C). The sensitivity of such fits to the low-temperature values of $\Delta G_U(T,0)$ and its errors, as well as the importance of determining $\Delta G_U(T,0)$ at the lowest possible temperatures, has been emphasized in earlier reports (*5*, *29*). This was done to the extent possible in this study.

The procedure described above was extended to analysis of thermal denaturation data at lower urea concentrations (0−2 M) with LEM $\Delta G_U'(T)$ values included as the low-temperature points since these appear to be closer to those estimated independently by calorimetry (see below). In the presence of 2.5 and 3 M urea, cold denaturation could be observed over the entire low-temperature range employed, and so LEM $\Delta G_U'(T)$ values were not included in the analysis. Figure 3D shows the experimental data for each urea concentration and the individual best fits [the corresponding stability curves (*5*, *29*)] to eq 5 using initial guesses for T_m' as described earlier. The best fit parameter values are listed in Table 2 and show that in the range of 1−3 M urea $\Delta C_{p,U}'$ values are very similar to, though somewhat greater than, those in 0 M urea. For the range of 0−3 M urea, the average temperature-independent value for $\Delta C_{p,U}'$ is 0.98 ± 0.05 kcal mol^{-1} K^{-1}. This $\Delta C_{p,U}'$, T_m, and ΔH_m in 0 M urea (Table 2) and eqs 8−10 yield a T_h of 9.5 °C, where $\Delta H = 0$ and $T_s = 12.8$ °C where $\Delta S = 0$ and the temperature of maximum protein stability calculated is 3.2 kcal mol^{-1}.

Thermal Unfolding of 434 Cro As Determined by Differential Scanning Calorimetry. A straightforward analysis of DSC data requires the transitions to be reversible, typically verified by checking for superimposable DSC curves obtained in sequential scans for the same sample cooled in the calorimetric cells after each run. The DSC curves were reversible at all pH values that were studied, except at pH 6.0 where they are irreversible at the protein concentrations that were used (around 100 μM), as reported previously (*15*). This was the case even when the samples were saturated with nitrogen to minimize oxidation of the single Cys in 434 Cro and any consequent intermolecular disulfide bond formation.

Lowering the pH to improve reversibility is frequently accompanied by broadening of the DSC transitions and lowering of T_m (*19*, *24*−*26*, *36*−*39*). This was also seen with 434 Cro (Figure 4A). Decreasing the pH below 5 destabilizes the native protein, and at pH 2.0, the heat absorbance peaks completely disappear from the melting curve. Consistent with this, the CD spectrum and $[\Theta]_{222}$ characteristic of native 434 Cro at pH 6.0 and 25 °C persist up to pH 4.0; $[\Theta]_{222}$ is slightly lower at pH 3.0, while at pH 2.0, the characteristic helical CD signals are absent (data not shown) and the spectrum resembles that of thermally denatured 434 Cro (*15*). The pH 2.0 heat capacity curve is, in fact, typical for unfolded proteins; its shape closely matches that calculated from the protein's amino acid content (*32*), although the latter values are about 10% greater at each temperature. Such a discrepancy, also reported for other proteins, is probably the consequence of assuming that the unfolded protein is completely random in structure with all its constituent amino acids optimally hydrated and with no neighboring group interference as in the small model compounds.

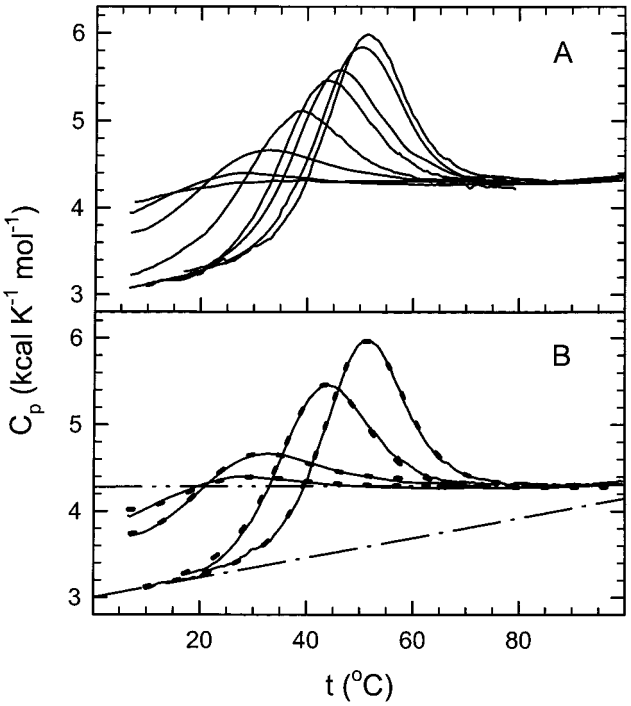

FIGURE 4: DSC data for 434 Cro at various pHs. (A) The temperature dependence of the partial molar heat capacity at pH 2.0, 2.65, 3.0, 3.5, 3.75, 4.0, 4.5, and 5.0 (from left to right according to increasing stability). All solutions contained 100 mM KCl and 20−25 mM sodium glycine (pH 2−4) or acetate or phosphate (pH 4−6). (B) The results (dotted lines) of the multiple best fit based on eqs 11−16 are shown for four curves selected from panel A (solid lines). The dash−dot lines show the best fit $C_{p,N}$ and $C_{p,U}$ linear functions common for all curves in this figure: $C_{p,N} = 2.99 + 0.012t$(°C) and $C_{p,U} = 4.18 + 0.0002t$(°C) both in kcal K^{-1} mol^{-1}.

The heat capacity of the native protein, $C_{p,N}$, increases with temperature, while that for the unfolded state, $C_{p,U}$, shows almost no such dependence (Figure 4A). The simplest approach to DSC data analysis is based on linear approximations for the temperature dependences of both $C_{p,N}$ and $C_{p,U}$

Table 3: Analysis of DSC Data of 434 Cro at Various pHs

	A[a]		B[a]		C[a]		
pH	T_m (°C)	ΔH_m (kcal mol^{-1})	T_m (°C)	ΔH_m (kcal mol^{-1})	T_s (°C)	$\Delta G_{U,max}$ (kcal mol^{-1})	ΔG_U(25 °C) (kcal mol^{-1})
2.65[b]	–	–	–	–	7.0 ± 0.2	−0.72 ± 0.2	−1.36 ± 0.2
3.00[b]	–	–	–	–	7.6 ± 0.1	0.02 ± 0.2	0.57 ± 0.2
3.50	32.6 ± 2.0	27.5 ± 3.0	32.9 ± 2.0	27.2 ± 2.4	8.5 ± 0.05	1.08 ± 0.1	0.55 ± 0.1
3.75	39.5 ± 1.0	32.4 ± 2.4	40.5 ± 1.0	32.9 ± 2.4	9.1 ± 0.05	1.77 ± 0.1	1.29 ± 0.1
4.00	41.9 ± 1.0	32.5 ± 2.4	42.7 ± 1.0	32.6 ± 2.4	9.2 ± 0.05	2.03 ± 0.1	1.55 ± 0.1
4.50	47.4 ± 0.5	37.6 ± 2.4	47.1 ± 0.5	36.3 ± 2.4	9.7 ± 0.05	2.49 ± 0.1	2.03 ± 0.1
5.00	49.0 ± 0.5	39.9 ± 2.4	49.1 ± 0.5	39.3 ± 2.4	9.8 ± 0.05	2.65 ± 0.1	2.20 ± 0.1
6.00	57.2 ± 0.5[c]	45.5 ± 4.0[d]	–	–	10.7 ± 0.1	3.66 ± 0.2	3.23 ± 0.2

[a] Individual curve fittings based on $\Delta H_m/T_m$ equations with linear (column A) and quadratic (column B) $C_{p,U}(T)$ functions. Column C lists the results of multiple fitting based on T_h/T_s equations with linear $C_{p,U}(T)$, a T_h of 7.6 °C, and a $\Delta G_{U,max}$ of $\Delta G(T_s)$ at 25 °C (see the text). [b] Fitting of these DSC data using $\Delta H_m/T_m$ equations not possible because the population of the native state is ≤0.5 at any temperature. [c] T_m estimated from the irreversible DSC curve. [d] Extrapolated value using eq 22.

and consequently $\Delta C_{p,U}$. This works well for curves with a T_m of >40 °C, since the nonlinearity of $C_{p,U}$ is known to be noticeable only below this temperature (*32*, *40*). Therefore, the linear approximation of $\Delta C_{p,U}$ was used throughout this study for both individual and multiple-DSC curve fitting. Some of the DSC curves for 434 Cro are broad and exhibit clear heat capacity changes below 40 °C. So we also checked if a nonlinear approximation of the baselines could alter the curve fittings. For this, the quadratic term coefficient (=0.93 × 10^{-4} kcal K^{-3} mol^{-1}) was determined using a second-order regression through the curve obtained at pH 2. A nonlinear temperature dependence was also assumed for $C_{p,N}$ since that for $C_{p,U}$ has been attributed to the temperature dependences of the heat capacities of hydrophilic groups exposed to water (*32*, *40*).

The algorithms based on the C_p curve fitting (without previous separation of the excess heat capacity, $C_{p,exc}$) give for each curve a unique ΔH_m value that is equal to the calorimetric and van't Hoff heat effects. A separate determination of the calorimetric and van't Hoff enthalpies cannot be reliably achieved for small proteins such as 434 Cro, because of their broad transitions and, hence, small unfolding enthalpies (*24*, *25*). Instead, two-state behavior was inferred from the quality of the fits of the DSC data to the two-state model. Another problem arises from the baseline uncertainty caused by low structure stability and a not so insignificant population of the unfolded species at any temperature. In fact, the entire set of experimental data presented in Figure 4A can be adequately analyzed only by a multiple-curve fitting where the baselines are assumed to be the same for all curves in the set. Figure 4B shows the result of such a fitting with the common best fit baselines using the T_h/T_s equations (eqs 13−16) for four of the DSC curves.

Table 3 lists the unfolding parameters determined using linear and quadratic baselines in single- and multiple-curve fitting of the DSC data. The corresponding ΔH_m versus T_m plot is shown in Figure 5. The DSC experiments reveal a sharp drop in protein stability in the acidic pH range. Such effects are typically entropic (electrostatic) in origin. Small heat effects that might accompany unfolding in the acidic pH range as a result of proton transfer are nearly fully offset by the approximate equivalence of the ionization enthalpies of the buffers and the protein acidic groups (*19*, *30*, *41*, *42*). The observed ΔH_m values thus reflect the true unfolding enthalpies, and $\Delta C_{p,U}$ can be evaluated using the Kirchhoff relation: $\Delta C_p = [\partial(\Delta H)/\partial(T)]_p$ from plots of ΔH_m versus

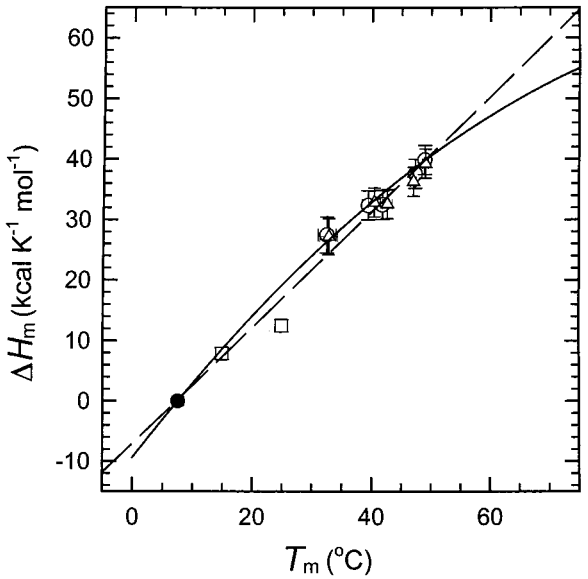

FIGURE 5: Plot of ΔH_m vs T_m with the ITC and multiple-fit data included. The white circles and white triangles correspond to the data listed in columns A and B of Table 3, respectively. White squares are unfolding enthalpies at 15 and 25 °C determined by isothermal titration calorimetry as described in the text. The black circle corresponds to the point where $\Delta H_U(T_h) = 0$ as determined by multiple-curve fitting. The dashed line shows a linear regression through all data points present in the figure (see eq 20). The solid line corresponds to eq 22 as determined by multiple-DSC curve fitting.

T_m (*5*, *10*, *26*). The small size and the relatively low stability of 434 Cro allow reliable determination of ΔH_m over only a narrow temperature range. This decreases the quality of the regression analysis and increases the magnitudes of the errors associated with $\Delta C_{p,U}$ and ΔG_U. To overcome this problem, the unfolding heat effect at lower temperatures was obtained from pH-induced unfolding monitored by ITC. The multiple-curve fitting of DSC data, in addition, directly yields T_h which can serve as a reliable reference for the low-temperature range. Inclusion of these additional data in the ΔH_m versus T_m plot clearly helped to improve the quality of the linear regression analysis.

As seen from Table 3, introducing nonlinear baselines causes only slight changes in the single-curve best fit parameters. This suggests that deviations of the baselines from linearity are not great, and/or that ΔH_m rather than C_p is the most important parameter in defining the shape and height of any particular C_p peak. The linear regression

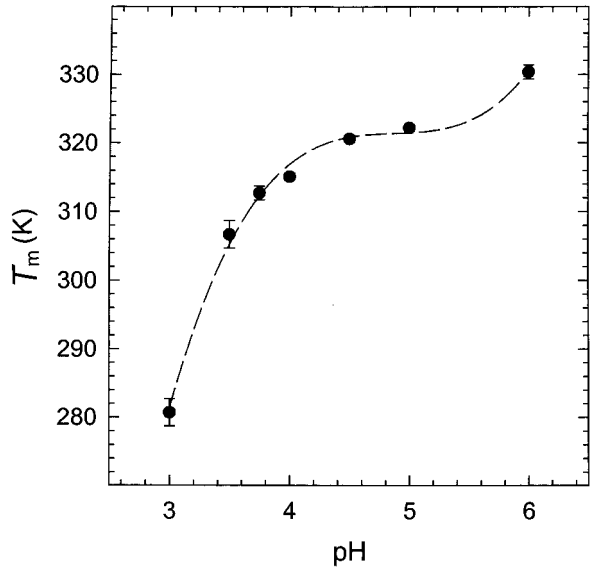

FIGURE 6: Plot of T_m vs pH of the data taken from Table 3. Since for the curve at pH 3.0 T_s coincides with T_h, these two correspond to T_m. The minimal-order polynomial used which adequately fits all the data on the graph is $T_m = -366 + 421.8(pH) - 86.4(pH)^2 + 5.9(pH)^3$. The derivative of this polynomial and the data from Table 3 were used to estimate the number of protons exchanged upon unfolding as defined in eq 23.

through all data points in Figure 5 (shown by the dashed line in this figure) corresponds to the following equation:

$$\Delta H_U(\text{kcal mol}^{-1}) = -7.1 + 0.95t(°\text{C}) \quad (20)$$

This corresponds to a constant $\Delta C_{p,U}$ of 0.95 ± 0.03 kcal mol^{-1} K^{-1}. Multiple-curve fitting based on the linear approximation of heat capacities yields the following equations from eqs 12 and 13 (when $T_r = T_h$):

$$\Delta C_{p,U}(\text{kcal mol}^{-1}\text{ K}^{-1}) = 1.19 - 0.0114(T - 280.73) \quad (21)$$

$$\Delta H_U(\text{kcal mol}^{-1}) = 1.19(T - T_h) - 0.0057(T - T_h)^2 \quad (22)$$

Equation 22 (not to be confused with a second-order regression through the data depicted in Figure 5) approximates very well the ΔH_m versus T_m data. According to eq 21, $\Delta C_{p,U}$ varies from 1.28 to 0.14 kcal K^{-1} mol^{-1} for the temperature range of 0−100 °C. At pH 6.0, where the DSC transition is irreversible, a fairly precise T_m of 57.2 ± 0.5 °C can nevertheless be estimated. This yields a ΔH_U of 45.5 kcal mol^{-1} (eq 22) or 47.2 kcal mol^{-1} (eq 20). From eqs 13, 14, and 21, ΔG_U(25 °C) is 3.23 ± 0.2 kcal mol^{-1}, or using the constant $\Delta C_{p,U}$ value given above, it is 3.07 kcal mol^{-1}.

The pH dependence of T_m (Figure 6) can be used to estimate $\Delta\nu$, the number of protons associated with protein unfolding (*29*, *41*).

$$\Delta\nu = \nu_U - \nu_N = (\Delta H_m/2.303RT_m^2)(dT_m/dpH) \quad (23)$$

where ν_U and ν_N are the number of protons bound to the denatured and native states, respectively. $\Delta\nu$ is estimated using the data in Table 3 and the slope at each pH determined from the derivative of a minimal-order polynomial which adequately fits all the data depicted in Figure 6. There is essentially no proton exchanging upon unfolding at pH 5 where the slope is nearly zero. The number of protons exchanging is about 1 at pH 4, and around 1.5 at pH 3.25 (maximum observed slope). The slope appears to increase above pH 5.0, but the lack of additional data above this pH hampers any conclusive analysis of this region.

DISCUSSION

Structural Stability of 434 Cro. 434 Cro exhibits unfolding thermodynamics typical for a number of other small, globular proteins (*5*−*12*, *19*, *24*−*26*, *36*−*39*). Its thermal stabilities as characterized by its T_m values agree for both far-UV CD and calorimetric thermal transition data, while the thermodynamic stability described by the free energy of unfolding, ΔG_U, is modest even at pH 6.0. ΔG_U(25 °C) in 0 M urea from urea denaturation data analyzed with the denaturant binding model (DBM) is higher than with the linear extrapolation model (LEM) [as reported for some other proteins (*5*, *10*)]. ΔG_U from the multiple fitting of the DSC data lies between those from DBM and LEM. Overall, these ΔG_U values compare favorably with estimates from hydrogen exchange studies of the slowest exchanging amide protons (*15*). The experimental *m* values match well the predictions based on correlations with the change in solvent-accessible surface area upon unfolding (*43*) or from data for other helical peptides and proteins (*44*) as noted earlier (*15*).

The thermodynamic stability at any temperature can be determined using eq 5 once ΔH_m, T_m, and $\Delta C_{p,U}$ are known. These have been determined for 434 Cro in this study using calorimetry and, independently, by analyzing chemical and thermal denaturation data using different reported procedures. Far-UV CD thermal denaturation data in conjunction with urea denaturation LEM and DBM ΔG_U values yield temperature-independent $\Delta C_{p,U}$ values of 0.91 ± 0.05 and 0.71 ± 0.03 kcal mol^{-1} K^{-1}, respectively, in the absence of urea, while $\Delta C_{p,U}$ values determined in the presence of 1−3 M urea are essentially identical to one another and slightly higher than in 0 M urea. Increases in $\Delta C_{p,U}$ with urea concentration are small for some proteins such as ribonuclease A and hen egg white lysozyme (*4*), but are significantly greater for barnase (*45*). $\Delta C_{p,U}$ calculated directly from the multiple fitting of DSC curves is temperature-dependent as has been observed in calorimetric studies of a number of other proteins. The constant temperature-independent $\Delta C_{p,U}$ estimated from the linear slope of a plot of ΔH_m versus T_m (both obtained from DSC data) almost coincides with that from the far-UV CD thermal urea denaturation, and so the two yield essentially identical ΔG_U (25 °C) values. ΔG_U (25 °C) determined directly from the multiple-DSC curve fitting is somewhat higher. The level of correspondence between the far-UV CD chemical and thermal denaturation and calorimetric data is quite good given the assumptions and/or extrapolations involved in either determination as is clear from Table 4 which lists, for comparison, $\Delta C_{p,U}$ values determined for a number of other small proteins using the two independent methods. On a per residue basis, $\Delta C_{p,U}$ values for 434 Cro are about 14 cal mol^{-1} K^{-1} (far-UV CD thermal and LEM data), 12 cal mol^{-1} K^{-1} (far-UV CD thermal and DBM data), and 14 cal mol^{-1} K^{-1} (from the

Table 4: $\Delta C_{p,U}$ from Calorimetry and Chemical and Thermal Denaturation Data for Some Proteins

		calorimetry[b]		chemical and thermal denaturation[b]		
protein[a]	no. of residues	$\Delta C_{p,U}$	ΔC_p/residue	$\Delta C_{p,U}$	ΔC_p/residue	refs[c]
ribonuclease T1	104	1.34 ± 0.07	12.9	1.65 ± 0.20 (u)	15.9	*5*, *38*
barnase	110	1.70 ± 0.05	15.5	1.88 ± 0.70 (p)	17.1	*45*, *46*
ribonuclease A	124	1.09 ± 0.07	8.8	1.28 ± 0.20 (u)	10.3	*47*
Iso-1-CytC	108	1.37 ± 0.06	12.7	1.37 ± 0.06 (p)	12.7	*48*
Ov3 domain	56	0.74 ± 0.14	13.2	0.64 ± 0.11 (g,u)	11.4	*6*, *39*
Barstar	89	1.12 ± 0.24	12.6	1.46 ± 0.07 (g)	16.4	*8*, *49*
Sac7d	66	0.50 ± 0.02	7.6	0.86 ± 0.02 (g,u)	13.0	10
434 Cro	71	0.95 ± 0.30/1.01 ± 0.10	13/14	0.98 ± 0.05 (u)	13.8	this study

[a] Iso-1-CytC, iso-1-ferricytochrome; Ov3 domain, ovomucoid third domain. [b] $\Delta C_{p,U}$ in kilocalories per mole per kelvin. ΔC_p/residue in cal K^{-1} mol^{-1}. (g), (p), and (u) indicate data from GdnHCl, pH, and urea denaturation, respectively, combined with thermal denaturation. [c] The first reference corresponds to calorimetry and the second to chemical and thermal denaturation.

Table 5: Summary of the Thermodynamic Parameters for 434 Cro and Comparison with Those for R1−69 and λ_{6-85}

parameter	434 Cro[a]	R1−69[b]	λ_{6-85}[c]
T_m (°C)	57.0 ± 0.1/57.2 ± 1.0	70.7 ± 0.5	57.2 ± 0.1
ΔH_m (kcal mol^{-1})	46.6 ± 0.05/47.2 ± 3.0/45.5 ± 2.4	58.6 ± 2.4	68 ± 1
$\Delta C_{p,U}$ (kcal mol^{-1} K^{-1})	0.98 ± 0.05/0.95 ± 0.03 [1.28 − 0.0114*t*(°C)]	0.80 ± 0.02	1.44 ± 0.03
m (kcal M^{-1} mol^{-1})	0.99 ± 0.10	na	1.13 ± 0.02
ΔG_U(25 °C) (kcal mol^{-1})	3.05 ± 0.49/3.07 ± 0.3/3.23 ± 0.2	5.20 ± 0.40	4.30 ± 0.20
ΔG_U(max at $T = T_s$) (kcal mol^{-1})	3.2/3.39/3.66	5.8	4.6
$T_s = T_{max}$ (°C)	12.8/11.0/10.6	4.7	13.2

[a] The entries for 434 Cro are (in order) from far-UV CD chemical and thermal denaturation data, from linear extrapolation of DSC ΔH_m vs T_m data, and from multiple-T_s/T_h fitting of DSC data as obtained in this study for the conditions mentioned in the text. [b] DSC data at pH 7.0, 200 mM NaCl, and 20 mM PIPES (*19*). [c] Chemical denaturation data at pH 8.0, 100 mM KCl, 25 mM KH_2PO_4, and 99% D_2O (*9*).

calorimetric value at 25 °C), which are values similar to those reported for a number of other globular proteins (Table 4; see also refs *10*, *43*, and *50*). The experimental $\Delta C_{p,U}$ determined for 434 Cro lies in the range of 0.90−1.60 kcal mol^{-1} K^{-1} predicted for this protein (*15*) using known empirical correlations that link $\Delta C_{p,U}$ to the solvent accessible surface areas in the native and unfolded structures (*43*, *51*, *52*). Discrepancies among these predictions and with experimental values can be as much as 25% (*43*). The reasons for these discrepancies though not entirely clear (*12*, *26*) have been attributed to differences in accessible surface area calculations used in deriving the empirical correlations (*43*).

The stability of 434 Cro decreases with acid pH with a net uptake of about one to two protons at pH <4. This must be due to one or two groups which in the native state are shielded from solvent and thereby from protonation, but which upon unfolding in acid pH take up protons (*29*). These groups must therefore have low pK_as in the native state relative to those in the denatured state and probably involve one of the four Glu or the single Asp present in 434 Cro (there are no histidines). In model compounds, pK_as for Glu cluster around 4.5 and 4 for Asp (*53*). Shielding of these acidic groups from solvent could occur by the formation of buried salt bridges. Indeed, such a salt bridge is present in native 434 Cro between Glu37 and Arg12, both of which have low solvent accessibilities [the other acidic residues are significantly more exposed to solvent (*14*, *15*)]. The consequent lowering of the pK of Glu37 could account for the essentially complete unfolding by pH 2.0.

Comparison of the Stabilities of 434 Cro with the N-Terminal Domains of 434 (R1−69) and λ Repressor (λ_{6-85}). 434 Cro and the N-terminal domains of 434 (R1−69) and λ repressor (λ_{6-85}) are remarkably similar in structure. Their sequences are also considerably similar to those of 434 Cro and R1−69, in particular, exhibiting almost 50% sequence identity. Table 5 lists the parameters describing their thermodynamic stabilities. For 434 Cro, parameters obtained in this study using chemical and thermal denaturation as well as calorimetry are listed. Those listed for R1−69 are from calorimetry (*19*) and for λ_{6-85} from chemical denaturation data (*9*), since these, to our knowledge, are the only ones available [the λ repressor N-terminal fragment (residues 1−92) has been studied calorimetrically but tends to dimerize at high concentrations; see ref *54*]. $\Delta C_{p,U}$ values for 434 Cro and R1−69 are closer to one another, not surprising given their near-identical structures and the correlation of $\Delta C_{p,U}$ with structure (*42*−*44*, *51*, *52*); the five helices in both proteins are equally long, and the backbone conformations of their structurally well-defined regions are almost exactly superimposable (*15*, *16*). Relative to those for 434 Cro and R1−69, $\Delta C_{p,U}$ for λ_{6-85} is larger, possibly due to its larger size (80 residues vs 71 for 434 Cro and 69 for R1−69), the longer lengths of helices 1 and 4 of its five helices [by three and two residues, respectively, compared to those in 434 Cro and in R1−69 (*16*)], and the consequent structural variations.

T_m for R1−69 is considerably higher than for λ_{6-85} or for 434 Cro, the latter also having the lowest ΔH_m. For several small proteins, it has been observed that a high T_m does not necessarily imply an unusally high stability, i.e., large ΔG_U values, but stems as a direct thermodynamic consequence from these proteins typically having small $\Delta C_{p,U}$ and ΔH_m values (*7*, *10*, *29*, *36*, *50*). The thermodynamic stabilities of 434 Cro, R1−69, and λ_{6-85} lie within the range observed for such small globular proteins. The maximum ΔG_U estimated assuming a constant $\Delta C_{p,U}$ is lowest for 434 Cro and highest for R1−69 (Table 4), the two differing by around 2 kcal mol^{-1} [ΔG_U values listed for λ_{6-85} are obtained in D_2O and exceed those in H_2O by ∼0.5 kcal mol^{-1} at 37 °C

(*9*)]. This is striking given the high degrees of sequence and structural similarity between 434 Cro and R1−69. Amino acid substitutions that enhance intrinsic helix stabilities have been shown to stabilize λ_{6-85} (*55*). Intrinsic helix stabilities in 434 Cro are low, but are predicted to be even lower for R1−69 (*56*), indicating that this may not be the basis for the higher stability of R1−69. Tertiary and packing interactions are more important determinants of protein stability. Sauer and co-workers have shown elegantly that the stability of the dimeric Arc repressor protein (another helix−turn−helix DNA-binding protein) is enhanced when buried salt bridge-forming residues are replaced with nonpolar residues that are compatible with steric and hydrogen-bonding requirements in the tertiary structure (*57*). This suggests that buried salt bridges could lower a protein's stability. 434 Cro does have a buried salt bridge (Arg12−Glu37) as mentioned earlier which may account for its lower stability. Although this salt bridge in 434 Cro does not have its counterpart in the more stable λ_{6-85} (*16*) or its variants (*56*), it is present in R1−69 (*16*, *17*). The reasons for the higher stability of R1−69 relative to 434 Cro (or to λ_{6-85}) probably lie elsewhere and remain to be established.

434 Cro, R1−69, and λ_{6-85} are monomeric even at the high concentrations used for crystallographic and NMR studies (*15*−*18*). Unlike 434 Cro which is the entire protein, R1−69 and λ_{6-85} constitute a specific single domain, the N-terminal domain, of the larger dimeric repressor. The stability of the domain in the context of the whole protein could thus be different relative to that in isolation because of cooperative effects from the rest of the molecule and in the dimer. Both R1−69 and residues 1−92 of the λ repressor can be generated by limited proteolysis using a relatively nonspecific protease, papain (*16*, *54*), suggesting these are independent structural units in the intact protein. Intact λ repressor has two distinct thermal transitions, one of which corresponds to that seen with the isolated N-terminal domain indicating that the latter is an autonomously folded unit with a stability similar to that of this domain in the intact protein (*54*). In dimeric constructs linking the flexible C-terminal tails of two R1−69 units or the C-terminal tail of one unit to the N-terminus of the other, the folding and stability of each R1−69 unit were found to be independent (*19*). Thus, the structural stabilities observed for isolated R1−69 and λ_{6-85} very likely carry over into the intact repressor, where they continue to be higher than that for 434 Cro.

A higher structural stability of a protein aids in its resistance to degradation by proteolysis and is, therefore, an important determinant of its in vivo stability and, thereby, concentration (*58*). Intracellular protein degradation and turnover is, of course, a complex process, and various other factors including the nature of the N- and C-terminal amino acids and sequences, intracellular salt and osmolyte concentrations, DNA binding, and the intricate cellular protein degradation machinery all come into play in modulating protein concentrations in vivo (*10*, *53*, *58*). We have observed that expression levels for R1−69 are greater than for 434 Cro in the same overexpression system and *E. coli* strain, consistent with R1−69 being more stable than 434 Cro in vivo (unpublished observation). In the case of phage λ, the stabilities of a putative folded monomeric form of its Cro protein and variants including a stable engineered monomer were recently reported (*59*). It was suggested that this folded monomeric λ Cro is sufficiently stable to be substantially populated relative to the dimer under conditions used for the formation of DNA-bound complexes in contrast to earlier studies where only stable dimers or unstructured monomers of λ Cro were presumed to exist (*59*). Furthermore, monomeric λ Cro was proposed to exist in vivo at substantial levels and its degradation linked to maintaining its concentrations within certain thresholds (*59*). The reported stability of the monomeric λ Cro is significantly lower than that of the λ repressor N-terminal domain, and is close to or lower than that of 434 Cro. The lower structural stability of the Cro protein relative to the N-terminal domain of the repressor (and possibly the intact repressor) observed in phages 434 and λ may therefore constitute a general and important role in regulating the relative intracellular concentrations of this protein pair and in fine-tuning the lysis versus lysogeny decision in the life cycle of the phage.

ACKNOWLEDGMENT

S.P. is indebted to Dr. S. Subbiah (Wistar Institute, University of Pennsylvania, Philadelphia, PA) for recommending 434 Cro as a model system and to him and the laboratory of Professor Steve Harrison (Harvard University, Cambridge, MA) for the gift of plasmids. We are grateful to Professors F. J. Murillo and F. Solano (Universidad de Murcia) and to Professor G. Giménez-Gallego and the Protein Chemisty division of CIB-Madrid for generous access to space and instrumental facilities and to Apolo Gómez and Christina López for technical assistance.

REFERENCES

1. Schellman, J. A. (1987) *Annu. Rev. Biophys. Biophys. Chem. 16*, 115−137.
2. Santoro, M. M., and Bolen, D. W. (1992) *Biochemistry 31*, 4901−4907.
3. Tanford, C. (1970) *Adv. Protein Chem. 21*, 1−95.
4. Makhatadze, G. I., and Privalov, P. L. (1992) *J. Mol. Biol. 226*, 491−505.
5. Pace, C. N., and Laurents, D. V. (1989) *Biochemistry 28*, 2520−2525.
6. Swint, L., and Robertson, A. D. (1993) *Protein Sci. 2*, 2037−2049.
7. Scholtz, J. M. (1995) *Protein Sci. 4*, 35−43.
8. Agashe, V. R., and Udgaonkar, J. (1995) *Biochemistry 34*, 3286−3299.
9. Huang, G. S., and Oas, T. G. (1996) *Biochemistry 35*, 6173−6180.
10. McCrary, B. S., Edmondson, S. P., and Shriver, J. W. (1996) *J. Mol. Biol. 264*, 784−805.
11. Yi, Q., Scalley, M. L., Simons, K. T., Gladwin, S. T., and Baker, D. (1997) *Folding Des. 2*, 271−280.
12. Kuhlman, B., and Raleigh, D. P. (1998) *Protein Sci. 7*, 2405−2412.
13. Ptashne, M. (1986) *A Genetic Switch: Gene control and phage λ*, Cell Press and Blackwell Scientific Publications, Cambridge, MA.
14. Mondragon, A., Wolberger, C., and Harrison, S. C. (1989) *J. Mol. Biol. 205*, 179−188.
15. Padmanabhan, S., Jiménez, M. A., González, C., Sanz, J. M., Giménez-Gallego, G., and Rico, M. (1997) *Biochemistry 36*, 6424−6436.
16. Mondragon, A., Subbiah, S., Almo, S. C., Drottar, M., and Harrison, S. C. (1989) *J. Mol. Biol. 205*, 189−200.
17. Neri, D., Billeter, M., and Wüthrich, K. (1992) *J. Mol. Biol. 223*, 743−767.

18. Huang, G. S., and Oas, T. G. (1995) *Biochemistry 34*, 3884−3892.
19. Ruiz-Sanz, J., Simonscits, A., Törö, I., Pongor, S., Mateo, P. L., and Filimonov, V. V. (1999) *Eur. J. Biochem. 263*, 246−253.
20. Studier, F. W., Rosenberg, A. H., Dunn, J. J., and Dubendorff, J. W. (1990) *Methods Enzymol. 185*, 60−89.
21. Gill, S. C., and von Hippel, P. H. (1989) *Anal. Biochem. 182*, 319−326.
22. Pace, C. N., Vajdos, F., Fee, L., Grimsley, G., and Gray, T. (1995) *Protein Sci. 4*, 2411−2423.
23. Pace, C. N., Shirley, B. A., and Thomson, J. A. (1990) in *Protein Structure: A Practical Approach* (Creighton, T. E., Ed.) pp 311−330, IRL Press, Oxford, England.
24. Viguera, A. R., Martínez, J. C., Filimonov, V. V., Mateo, P. L., and Serrano, L. (1994) *Biochemistry 33*, 2142−2150.
25. Martinez, J. C., Viguera, A. R., Serrano, L., Filimonov, V. V., and Mateo, P. L. (1998) *React. Funct. Polym. 36*, 221−225.
26. Filimonov, V. V., Azuaga, A. I., Viguera, A. R., Serrano, L., and Mateo, P. L. (1999) *Biophys. Chem. 77*, 195−208.
27. Izzat, R. M., and Christensen, J. J. (1968) *Handbook of Biochemistry*, Rubber Co., Cleveland, OH.
28. Pace, C. N. (1986) *Methods Enzymol. 131*, 266−280.
29. Becktel, W. J., and Schellman, J. A. (1987) *Biopolymers 26*, 1859−1877.
30. Privalov, P. L. (1990) *Crit. Rev. Biochem. Mol. Biol. 25*, 281−305.
31. Privalov, P. L., and Potekhin, S. A. (1986) *Methods Enzymol. 131*, 4−51.
32. Makhatadze, G. I., and Privalov, P. L. (1990) *J. Mol. Biol. 213*, 375−384.
33. Rohl, C. A., and Baldwin, R. L. (1997) *Biochemistry 36*, 8435−8442.
34. Chen, B., and Schellman, J. A. (1989) *Biochemistry 28*, 685−691.
35. Yao, M., and Bolen, D. W. (1995) *Biochemistry 34*, 3771−3781.
36. Alexander, P., Fahnestock, S., Lee, T., Orbn, J., and Bryan, P. (1992) *Biochemistry 31*, 3597−3603.
37. Martínez, J. C., El Harrous, M., Filimonov, V. V., Mateo, P. L., and Fersht, A. R. (1994) *Biochemistry 33*, 3919−3926.
38. Yu, Y., Makhadatze, G. I., Pace, C. N., and Privalov, P. L. (1994) *Biochemistry 33*, 3312−3319.
39. Swint-Kruse, L., and Robertson, A. D. (1995) *Biochemistry 34*, 4724−4732.
40. Privalov, P. L., Tiktopulo, E. I., Venyaminov, S. Y., Griko, Y. V., Makhadatze, G. I., and Khechinashvili, N. N. (1989) *J. Mol. Biol. 205*, 737−750.
41. Privalov, P. L. (1979) *Adv. Protein Chem. 33*, 167−241.
42. Gómez, J., and Friere, E. (1995) *J. Mol. Biol. 252*, 337−350.
43. Myers, J. K., Pace, C. N., and Scholtz, J. M. (1995) *Protein Sci. 4*, 2138−2148.
44. Scholtz, J. M., Barrick, D., York, E. J., Stewart, J. M., and Baldwin, R. L. (1995) *Proc. Natl. Acad. Sci. U.S.A. 92*, 185−189.
45. Johnson, C. M., and Fersht, A. R. (1995) *Biochemistry 34*, 6795−6804.
46. Oliveberg, M., Vuilleumier, S., and Fersht, A. R. (1994) *Biochemistry 33*, 8826−8832.
47. Pace, C. N., Grimsley, G. R., Thomas, S. T., and Makhadatze, G. I. (1999) *Protein Sci. 8*, 1500−1504.
48. Cohen, D. S., and Pielak, G. J. (1994) *Protein Sci. 3*, 1253−1260.
49. Schöppe, A., Hinz, H.-J., Agashe, V. R., Ramachandran, S., and Udgaonkar, J. B. (1997) *Protein Sci. 6*, 2196−2202.
50. Privalov, P. L., and Gill, S. (1988) *Adv. Protein Chem. 39*, 191−234.
51. Spolar, R. S., Livingstone, J. R., and Record, M. T., Jr. (1992) *Biochemistry 31*, 3947−3955.
52. Murphy, K. P., and Friere, E. (1992) *Adv. Protein Chem. 43*, 313−361.
53. Creighton, T. E. (1993) in *Proteins*, W. H. Freeman and Co., New York.
54. Sauer, R. T., Jordan, S. R., and Pabo, C. O. (1990) *Adv. Protein Chem. 40*, 1−61.
55. Burton, R. E., Huang, G. S., Daugherty, M. A., Calderone, T. L., and Oas, T. G. (1997) *Nat. Struct. Biol. 4*, 305−310.
56. Padmanabhan, S., Jiménez, M. A., and Rico, M. (1999) *Protein Sci. 8*, 1675−1688.
57. Waldburger, C. D., Schildbach, J. F., and Sauer, R. T. (1995) *Nat. Struct. Biol. 2*, 122−128.
58. Parsell, D. A., and Sauer, R. T. (1989) *J. Biol. Chem. 264*, 7590−7595.
59. Jana, R., Hazbun, T. R., Mollah, A. K. M. M., and Mossing, M. C. (1997) *J. Mol. Biol. 273*, 402−416.

BI991757+